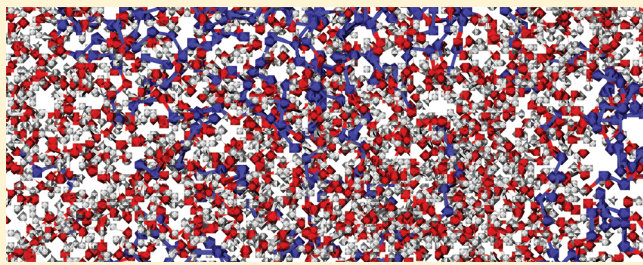


Association and Microheterogeneity in Aqueous 2-Butoxyethanol Solutions

Rini Gupta and G. N. Patey*

Department of Chemistry, University of British Columbia, Vancouver BC, Canada, V6T 1Z1

ABSTRACT: Molecular dynamics simulations are employed to investigate aggregation and microheterogeneity in dilute solutions of 2-butoxyethanol (BE) in water. The BE concentration is varied from near infinite dilution to the mole fraction $X_{\text{BE}} = 0.04$. It was found that large systems (32 000 molecules) are necessary to accommodate the BE aggregates that form in this concentration range. Simulations were performed with two different force fields, and similar results were obtained. At very low concentration, BE aggregation is not observed, but evidence is found for intramolecular hydrogen bonds (between the hydroxyl hydrogen and the ether oxygen of the same BE molecule) that form five-member ring configurations, similar to those reported in experimental studies of BE in nonaqueous solvent. Initial signs of BE association appear at $X_{\text{BE}} \approx 0.005$, after which aggregation occurs rapidly, with aggregates that can be described as micelle-like being fully formed at $X_{\text{BE}} \approx 0.02$. This concentration agrees well with many experimental studies of aggregation in BE–water solutions. Between $X_{\text{BE}} = 0.02$ and 0.04, the aggregates appear to grow a little in size, but the basic structure remains the same. At long range, the various pair correlation functions show clear density oscillations associated with BE aggregation. This allows us to identify the length scales of the existing microheterogeneity and to estimate the size of the BE aggregates. If we assume spherical aggregates, then our estimate of the radius at $X_{\text{BE}} = 0.04$ ($\sim 42 \text{ \AA}$) is close to estimates obtained from light scattering and small-angle neutron scattering experiments.



I. INTRODUCTION

The physiochemical properties of aqueous solutions of small amphiphilic molecules, such as alcohols, alkoxy alcohols, amines, and others, can exhibit unusual behavior at relatively low concentrations.^{1–12} For such systems, particular features observed in both thermodynamic^{1–5} and spectroscopic^{6–12} measurements are often associated with the possible existence of some sort of species aggregation, characterized by a length scale that exceeds that of a single molecule. Such solutions are sometimes described as microheterogeneous, but the exact nature of the microheterogeneity has remained elusive in some systems, with aqueous *tert*-butyl alcohol (TBA) solutions being perhaps the best known example.⁶

More recently, there have been a number of computer simulation studies^{13–23} aimed at gaining insight into association and microheterogeneity in aqueous systems. Considerable progress has been made, and we note in particular the understanding that has been gained of methanol–water^{10,17,18} and ethanol–water²² solutions. However, issues and questions remain. At a basic level, it is not at all clear how to describe or even recognize microheterogeneity if well-defined aggregates or clusters cannot be easily identified. For example, there is experimental^{1,6,7,9} and simulation^{13–16} evidence for TBA association in dilute TBA–water systems, but a good description of the “associated state” has yet to emerge. Concentration fluctuations that are always present, especially so if there is a nearby demixing critical point, must also be considered, and might further confuse matters in some systems.²⁰

Additionally, computer simulations have “technical” questions related mainly to finite system size and finite simulation times. The system size should be larger than the largest length scale related to aggregation, and molecular dynamics (MD) simulations must be longer than the time required for any aggregates to form, and for the aggregated system to achieve equilibrium. While it is difficult to know these simulation parameters *a priori*, they can be subjected to empirical tests.

This paper is a contribution to the continuing effort to understand aqueous solutions where association and microheterogeneity are believed to be important at low concentration. We report a molecular dynamics simulation investigation of aqueous 2-butoxyethanol (BE, $\text{CH}_3-(\text{CH}_2)_3-\text{O}-(\text{CH}_2)_2-\text{OH}$) solutions. BE–water solutions have been studied extensively by a variety of experimental methods, and many physical properties have been shown to undergo rather dramatic changes on variation of composition and temperature.^{1,3–5,8,24–50} In particular, for BE–water solutions, densities,^{25–27} refractive indices,²⁶ surface tensions,^{28–30} excess molar volumes,^{25,35} ultrasonic speeds,^{37,38} vapor pressures,³¹ heat capacities,^{4,25,28} and excess thermodynamic properties^{1,4,5,32–36} have been reported. We note that, in addition to the usual partial molar properties, Koga and co-workers^{1,4,5,32,34} have obtained so-called “third¹ and fourth⁵

Received: October 14, 2011

Revised: November 9, 2011

Published: November 14, 2011

Table 1. Lennard-Jones Parameters and Partial Charges for the Models Considered^a

atom	σ (Å)	ϵ (kJ/mol)	charge (e)
water (SPC/E)			
O	3.166	0.6501	-0.8476
H	0.0	0.0	0.4238
water (TIP3P)			
O	3.1505	0.63638	-0.834
H	0.0	0.0	0.417
BE (GROMOS G53A6 UNITED-ATOM)			
methyl group	3.7479	0.86715	-0.108
CH ₂ (1)	4.0704	0.41054	0.194
CH ₂ (2)	4.0704	0.41054	0.143
CH ₂ (3)	4.0704	0.41054	-0.035
CH ₂ (4)	4.0704	0.41054	0.151
CH ₂ (5)	4.0704	0.41054	0.231
O (ether)	2.8492	1.05711	-0.345
O (hydroxyl)	2.9548	0.84961	-0.617
H (hydroxyl)	0.0	0.0	0.386
BE (CHARMM27 ALL-ATOM)			
C(methyl),C1,C2	3.8754	0.2301	0.0
C3,C4,C5	3.8754	0.2301	0.28
O (ether)	3.1537	0.6364	-0.56
O (hydroxyl)	3.1537	0.6364	-0.68
H (hydroxyl)	0.40	0.19246	0.40
H (alkyl groups)	2.3519	0.09204	0.0

^a The methylene carbon atoms are denoted C1–C5, with the location labels as shown: CH₃—CH₂(1)—CH₂(2)—CH₂(3)—O—CH₂(4)—CH₂(5)—OH.

derivative” quantities, which provide strong signals of unusual behavior in BE–water and other aqueous systems. Also, the structure of BE–water systems has been directly probed by means of light scattering,^{41–47} and small-angle neutron scattering (SANS) experiments.^{12,48,49} In most of the studies cited above, some measured property of BE–water solutions is observed to change rapidly at some particular concentration, for example, at a BE mole fraction (X_{BE}) in the neighborhood of 0.02 at 298 K. This feature has been widely associated with the formation of BE aggregates that have been described as micelle-like,⁴³ or as pseudomicelles.⁵⁰ However, from a microscopic perspective, much remains to be learnt about the formation and nature of the associated species in BE–water systems.

The present MD investigation has two objectives. First, BE–water solutions are interesting in their own right, and we wish to gain an understanding of the formation, growth, and structure of any aggregated species, as a function of concentration. Second, we look to identify some “measures” or “signatures” of microheterogeneity that might prove more general, and be useful for other systems. For the second objective, we believe that BE–water is a good system with which to begin. From information presently available, the BE–water system appears to form better defined aggregates than other small-molecule–water solutions, and one might expect this to help with the physical interpretation of the MD results.

The remainder of this paper is organized as follows. The models and simulation method are described in section II,

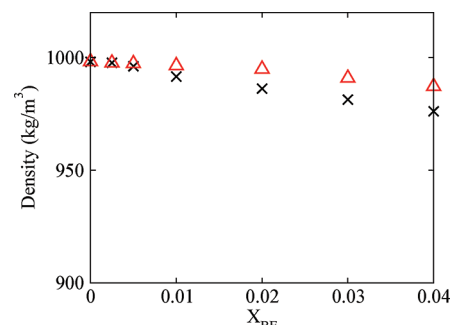


Figure 1. Variation of the density of BE–water solutions with X_{BE} . The triangles are experimental values,²⁶ and the crosses are the average densities obtained for the BE(GROMOS-UA)/water(SPC/E) model with 32 000 particles.

the results are presented and discussed in section III, and our conclusions are summarized in section IV.

II. MODELS AND SIMULATION METHOD

To ensure that our results are not an artifact of a particular model, simulations were performed with two different force fields. In one set of calculations, the SPC/E water model⁵¹ was combined with the GROMOS 53A6⁵² model for BE, and in the other the CHARMM27 model⁵³ was employed together with the TIP3P model⁵⁴ for water. In the GROMOS 53A6 model for BE, all alkyl groups are represented in the united atom (UA) approximation, whereas CHARMM27 BE is an all-atom (AA) model. We refer to these models as BE(GROMOS-UA)/water(SPC/E) and BE(CHARMM-AA)/water(TIP3P), respectively. In all molecular models the bond lengths and angles are held fixed. In both models, the atom–atom interactions are described by Lennard-Jones (LJ) and Coulombic interactions, and the relevant parameters are summarized in Table 1. The LJ cross interactions were obtained using the usual Lorentz–Berthelot combining rules.

Molecular dynamics (MD) simulations were carried out using GROMACS^{55,56} version 4.5.4 in double precision. The equations of motion were integrated using the leapfrog algorithm with a time step of 1 fs. The LJ interactions were cut off at 0.9 nm. The Coulombic interactions were treated using the particle mesh Ewald (PME) method.^{57,58} The real space interactions were evaluated using a 0.9 nm cutoff, and the reciprocal space interactions were calculated on a 0.12 nm grid with fourth order cubic spline interpolation. All the simulations were performed at constant temperature (300 K) and pressure (1 atm). The temperature was controlled using a velocity rescaling algorithm⁵⁹ ($\tau_t = 0.1\text{ps}$), and the pressure by applying the Berendsen coupling scheme⁶⁰ ($\tau_p = 1\text{ps}$). The molecules were kept rigid by applying constraints to the interatomic distances within a molecule, using the LINCS algorithm.⁶¹ Initial configurations for the simulations were obtained by minimizing the energy of water and BE molecules placed in a cubical box. The initial box sizes were determined from the experimental densities²⁶ of BE–water solutions. All systems were equilibrated for 2 ns, which was then followed by production runs of 8 ns. The results presented were obtained by averaging over configurations sampled during the production runs.

In order to investigate BE association and microheterogeneity, it proved necessary to carry out simulations with rather large

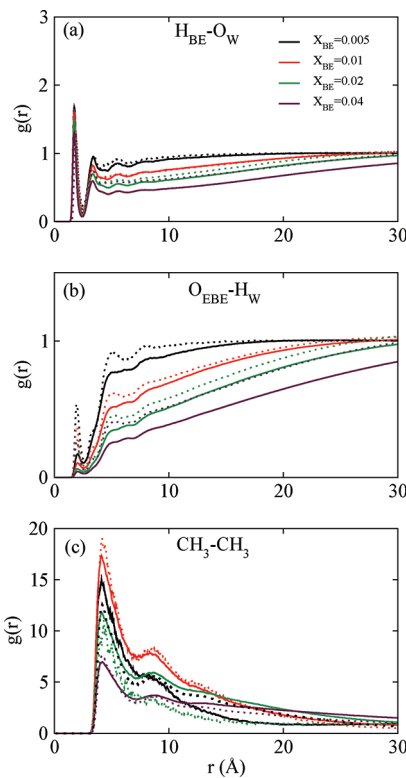


Figure 2. A comparison of selected rdfs for the BE(GROMOS-UA)/water(SPC/E) (solid lines) and BE(CHARMM-AA)/water(TIP3P) (dotted lines) models. The former were obtained with 32 000 particles and the latter with 8000, but the apparent differences are due to the different models; the results obtained with 32 000 and 8000 particles are not distinguishable on the scale used in the plot.

systems. For the BE(GROMOS-UA)/water(SPC/E) model, we report results for 8000 and 32 000 particles (water plus BE molecules), and for 8000 particles in the BE(CHARMM-AA)/water(TIP3P) case. The BE mole fractions, X_{BE} , considered are ~ 0 , 0.0025, 0.005, 0.01, 0.02, 0.03, and 0.04. Additionally, results were obtained for pure BE ($X_{BE} = 1.0$) using 2000 molecules, for comparison purposes.

III. RESULTS AND DISCUSSION

The average densities at 1 atm of the solutions we have simulated are compared with experimental data²⁶ in Figure 1. We note that both the model and experimental densities decrease with increasing X_{BE} , but that in general the densities of the model solutions are somewhat lower than the experimental values, especially at the higher mole fractions.

It would be interesting to further test our model by comparing with experimental data for excess molar thermodynamic functions, but at the low concentrations we consider, we do not have sufficient numerical accuracy for this to be meaningful. For example, over our concentration range the experimental excess molar enthalpies³⁵ vary from approximately -0.03 to -0.3 kJ mol $^{-1}$. In our simulations, we do obtain absolute enthalpies for the solutions as well as for the pure components, and therefore, in principle, we can calculate the excess values. The problem is that the absolute enthalpies involved are on the order of -40 kJ mol $^{-1}$ and larger, which means that even small uncertainties in these numbers lead to errors on the excess enthalpies that are larger

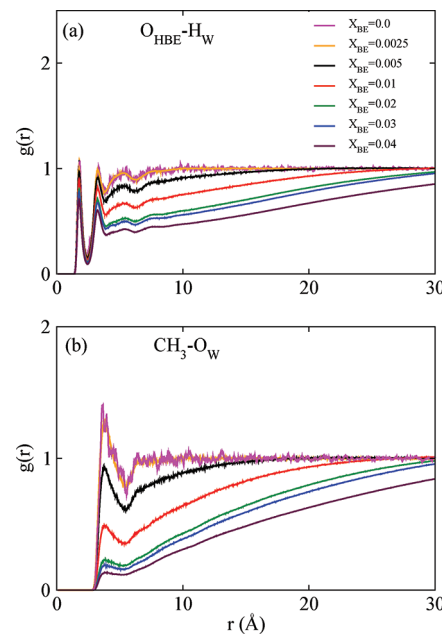


Figure 3. Selected BE–water rdfs obtained for the BE(GROMOS-UA)/water(SPC/E) model using 32 000 particles.

than the excess enthalpies themselves, much larger at low concentrations. This sensitivity to error makes any attempt at comparison with experiment meaningless; for different concentrations we get excess molar enthalpies that vary at random between -0.3 and $+0.3$ kJ mol $^{-1}$.

A. BE–Water and BE–BE Radial Distribution Functions. We have obtained atom–atom radial distribution functions (rdfs) for all possible solute–solute, solvent–solvent, and solute–solvent pairs, and here we show a selection to illustrate important points. In the figures and in our discussion, particular atoms are designated as follows: H_{BE} , the hydroxyl hydrogen of BE; O_{HBE} , the hydroxyl oxygen of BE; O_{EBE} , the ether oxygen of BE; CH_3 , the methyl group of BE; H_W , the hydrogen of water; and O_W , the oxygen of water. We first compare results obtained with the two different models considered.

As discussed above, these are the BE(GROMOS-UA)/water(SPC/E) and BE(CHARMM-AA)/water(TIP3P) models. Results obtained for selected BE–water and BE–BE rdfs at four concentrations are shown in Figure 2. We note that, while there are obvious quantitative discrepancies between the models, both give qualitatively similar results, and this is also true of the atom–atom rdfs not shown here. The rdfs compared in Figure 2 were selected because they are of particular importance; the O_W-H_{BE} and $O_{EBE}-H_W$ rdfs indicate only very weak hydrogen bonding between water hydrogen and the ether oxygen of BE. Since the physical picture of dilute BE–water solutions that emerges from both models is very similar, in the following discussion we focus mainly on the BE(GROMOS-UA)/water(SPC/E) model, for which we have carried out simulations of larger systems. However, results for the BE(CHARMM-AA)/water(TIP3P) model are included in some figures to further

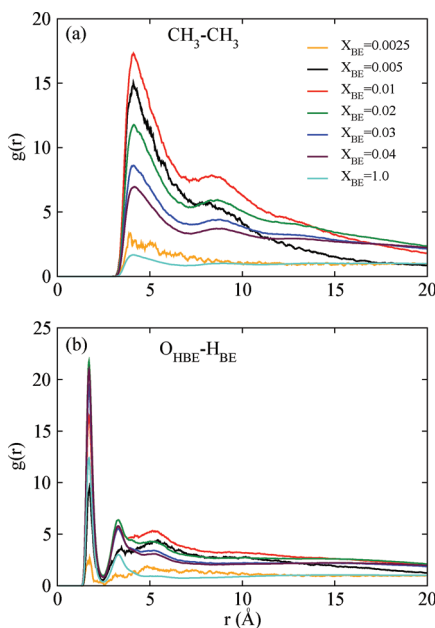


Figure 4. Selected BE–BE rdf s. All solution curves were obtained with the BE(GROMOS-UA)/water(SPC/E) model using 32 000 particles. The pure BE result was obtained with 2000 particles.

illustrate the overall qualitative agreement between the models as well as to illustrate certain features that show up more clearly in the all atom model.

Two additional BE–water rdf s, $O_{HBE}-H_W$ and CH_3-O_W , are shown in Figure 3 for a range of concentrations, including the near infinite dilution result ($X_{BE} = 1/32000$). The $H_{BE}-O_W$ rdf s shown in Figure 2 indicate hydrogen bonding with water acting as a proton acceptor; it is apparent from the $O_{HBE}-H_W$ rdf plots in Figure 3a that water can also act as a donor in BE–water hydrogen bonds. At infinite dilution, both rdf s shown in Figure 3 have initial short-range structure, but rapidly approach unity as the BE–water distance increases. It is interesting to note that, at very low concentration, the first peak in CH_3-O_W rises above one, indicating that even near the methyl group (which one would expect to be a hydrophobic part of BE) the water density exceeds the bulk value, if the BE concentration is sufficiently low. We see that at $X_{BE} = 0.0025$, the rdf s essentially coincide with the infinite dilution curves, but clearly discernible differences can be seen at $X_{BE} = 0.005$, and as the concentration is further increased the first peak in CH_3-O_W drops very rapidly, and both rdf s develop long-range tails approaching unity slowly from below. The long-range tails, and the remarkable concentration dependence of these rdf s, result from the aggregation of BE molecules. The nature of this aggregation is discussed below.

Selected BE–BE rdf s for concentrations ranging up to $X_{BE} = 0.04$ are shown in Figures 4 and 5. The pure BE ($X_{BE} = 1.0$) result is included for comparison purposes. From Figure 4, we see that for CH_3-CH_3 and $O_{HBE}-H_{BE}$ the initial peak is lowest for the lowest concentration considered ($X_{BE} = 0.0025$), and grows with increasing concentration until $X_{BE} \approx 0.01 - 0.02$, then decreases again toward the pure BE result as the concentration is further increased to $X_{BE} = 0.04$. This behavior, particularly the initial growth in peak height with increasing concentration, is also associated with BE aggregation. We note that the initial peak at $\sim 1.75 \text{ \AA}$ in $O_{HBE}-H_{BE}$ (Figure 4b) clearly indicates hydrogen

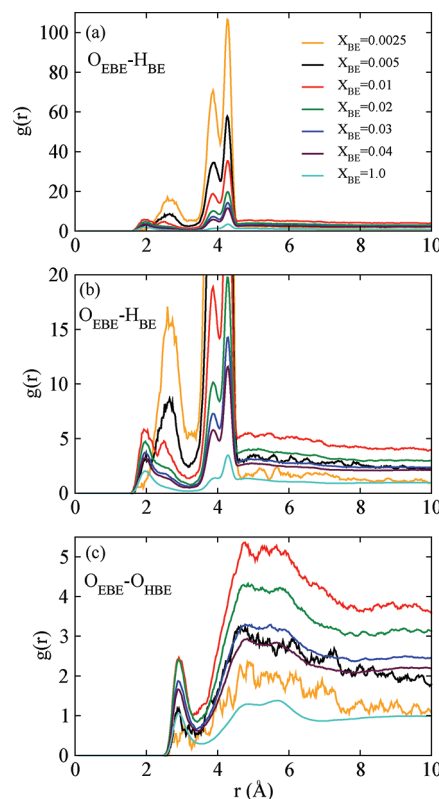


Figure 5. $O_{HBE}-H_{BE}$ and $O_{HBE}-O_{HBE}$ rdf s obtained for the BE(CHARM-M-AA)/water(TIP3P) model 8000 particles. Note that these particular rdf s contain both intra- and intermolecular contributions.

bonding of the BE hydroxyl groups, particularly at concentrations above $X_{BE} = 0.0025$.

Hydrogen bonding of the hydroxyl hydrogen and the ether oxygen of BE is interesting because there exists the possibility of both intra- and intermolecular hydrogen bonds, and, at least for dilute nonaqueous solutions, there is strong experimental evidence for both possibilities.⁶² Specifically, in dilute BE–CCl₄ solutions, there is evidence of equilibria among free (no hydrogen bonds), intramolecularly, and intermolecularly hydrogen-bonded BE species.⁶² The $O_{HBE}-H_{BE}$ and $O_{HBE}-O_{HBE}$ rdf s plotted in Figure 5 give an indication of the hydroxyl-hydrogen–ether-oxygen hydrogen bonding in the present model. In Figure 5 we show results for the BE(CHARM-M-AA)/water(TIP3P) model, because some structural features appear more clearly with the all atom model. It should be emphasized that the particular atom–atom rdf s shown in Figure 5 contain both intra- and intermolecular contributions.

First consider the $O_{HBE}-H_{BE}$ rdf s shown in Figure 5a, and on an expanded scale in Figure 5b. At very low concentration, this rdf will be completely dominated by intramolecular contributions, and at $X_{BE} = 0.0025$ only three peaks appear; an initial peak at $\sim 2.5 \text{ \AA}$, followed by two overlapping peaks near $\sim 4 \text{ \AA}$. This structure in the rdf is consistent with the situation found in dilute BE–CCl₄ solutions, where spectroscopic studies indicate an equilibrium between free and intramolecularly hydrogen-bonded BE molecules; the intramolecular hydrogen bond creates a five-member (atom) ring structure.⁶² At $X_{BE} = 0.0025$ the first peak in the rdf can be associated with five-member rings, and the second peaks with free BE molecules, with the closely overlapping peaks reflecting different molecular conformations. We note that the

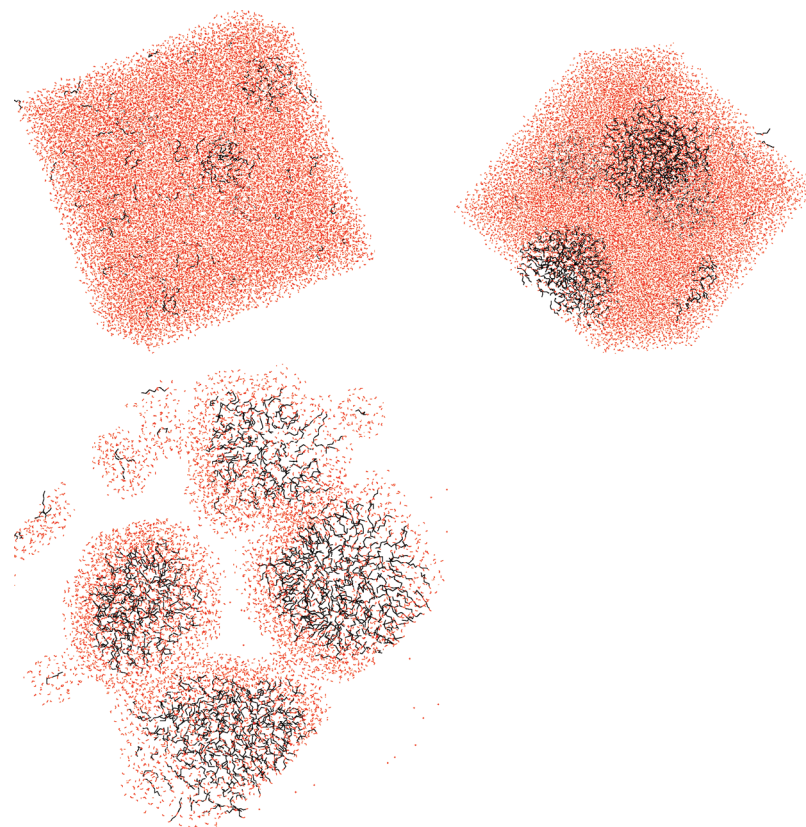


Figure 6. Configurational snapshots obtained for the BE(GROMOS-UA)/water(SPC/E) model with 32 000 particles. The water molecules are red and the BE molecules are black. The left panel is at $X_{BE} = 0.005$, and the right and lower panels are at $X_{BE} = 0.02$. In the lower panel, only water molecules within 5 Å of a BE molecule are shown.

position of the first peak at ~ 2.5 Å is larger than the separation normally associated with hydrogen bonding, but it is reasonably close to the hydrogen–oxygen distance in five-member rings (2.3 Å) estimated from BE–CCl₄ experiments.⁶²

As the concentration is increased we observe that another peak at ~ 1.9 Å appears in the O_{HBE}–H_{BE} rdfs. This peak grows in height with increasing concentration up to $X_{BE} \approx 0.01$, then decreases toward the pure BE result as the concentration is further increased. Given its position and concentration dependence, we associate this peak with intermolecular hydrogen bonding involving different BE molecules. Such intermolecular hydrogen bonds have also been detected in BE–CCl₄ solutions.⁶² The intramolecular hydrogen bond peak diminishes with increasing BE concentration, and appears only as a shoulder for $X_{BE} \gtrsim 0.02$, including pure BE.

The O_{EBe}–O_{HBE} rdfs (Figure 5c) gives a similar picture. At $X_{BE} = 0.0025$, the rdf has only a single broad peak that must include both free and intramolecularly hydrogen-bonded BE species. As the concentration is increased a peak related to intermolecular hydrogen bonding appears at ~ 2.8 Å.

B. BE Aggregation and Microheterogeneity. Above we noted features of the BE–water and BE–BE rdfs that are related to the aggregation of BE molecules. Qualitatively, a direct way of observing solute aggregation is to simply examine configurational “snapshots” such as those shown in Figure 6 for $X_{BE} = 0.005$, and 0.02. We see that, even at $X_{BE} = 0.005$, some BE–BE aggregation is discernible and that at $X_{BE} = 0.02$ fairly well-defined aggregates can be seen. These might be what earlier authors had in mind,

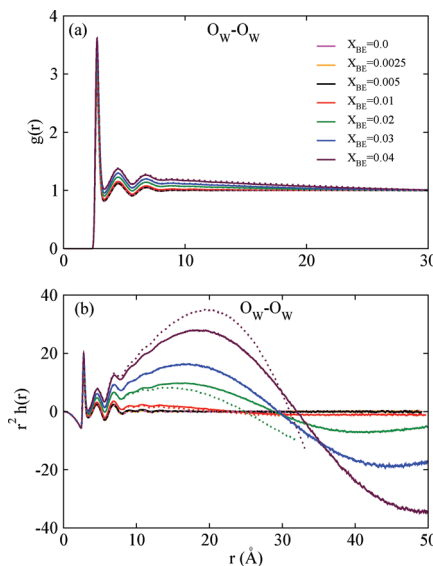


Figure 7. Water–water rdfs (a) and $r^2h(r)$ plots (b) obtained for the BE(GROMOS-UA)/water(SPC/E) model. The solid and dotted curves were obtained with 32 000 and 8000 particles, respectively.

when they interpreted their experimental observations for dilute BE–water solutions in terms of the formation of “micelle-like” entities⁴³ or “pseudomicelles”.⁵⁰ However, we note from the more expanded view at $X_{BE} = 0.02$ (Figure 6, lower panel) that

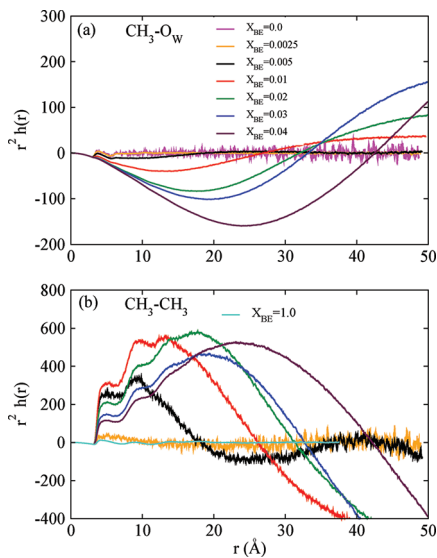


Figure 8. Plots of $r^2 h(r)$ for selected BE–water (a) and BE–BE (b) rdf. Note that the pure BE result is included in panel (b).

the BE aggregates are very loose structures and that there is a significant amount of water present in the BE-rich regions.

No matter how one chooses to describe the BE aggregates, it is clear that microheterogeneity, with water-rich and water-poor regions, develops in these solutions as the BE concentration is increased. A more quantitative description of the concentration dependence of the aggregation and of the length scales associated with the microheterogeneity can be obtained by examining the long-range behavior of the rdf. First, we consider the water–water correlations. The O_W-O_W rdf are plotted in Figure 7a, and for amplification purposes $r^2 h(r)$, where $h(r) = g(r) - 1$ is the pair correlation function, is shown in Figure 7b. We note that the first peak in the O_W-O_W rdf is not much influenced by increasing BE concentration, but that the rdf develop long-range tails as the BE concentration increases. The nature of the long-range behavior can be clearly seen in the $r^2 h(r)$ plot. For $X_{BE} \lesssim 0.005$, very little long-range structure can be detected, but at $X_{BE} = 0.01$ and higher concentrations, oscillations can be seen in $r^2 h(r)$. These oscillations in $r^2 h(r)$ indicate the presence of water-rich and water-poor regions. The amplitude of the oscillations increases with increasing BE concentration, and the position where $r^2 h(r)$ crosses zero varies from $\sim 20 \text{ \AA}$ at $X_{BE} = 0.01$, to $\sim 30 \text{ \AA}$ at $X_{BE} = 0.02$, then increases only a little as the concentration is increased to $X_{BE} = 0.04$. We note that $L/2$, where L is the length of the simulation cell, is concentration dependent, but is $\sim 32.5 \text{ \AA}$ for 8000 particles, and $\sim 50.5 \text{ \AA}$ for 32 000 particles, so clearly even at relatively low concentrations rather large systems are necessary to accommodate the length scales of the microheterogeneity associated with the BE aggregation.

Long-range oscillations also occur in all of the BE–water and BE–BE rdf. As examples, $r^2 h(r)$ results for CH_3-O_W and CH_3-CH_3 are plotted in Figure 8. At $X_{BE} = 0.005$, only a weak effect is discernible in the CH_3-O_W curve. However, the CH_3-CH_3 result (and other BE–BE rdf not shown) exhibit definite oscillations at $X_{BE} = 0.005$, indicating some association at this concentration, consistent with the configurational snapshot shown in Figure 6. The CH_3-CH_3 and other BE–BE rdf show no oscillation at $X_{BE} = 0.0025$, nor in pure BE ($X_{BE} = 1$).

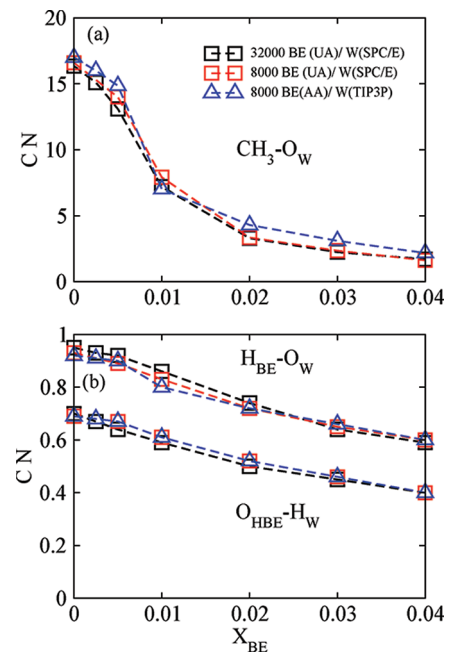


Figure 9. Selected BE–water coordination numbers. Results are included for both the BE(GROMOS-UA)/water(SPC/E) (8000 and 32 000 particles) and the BE(CHARMM-AA)/water(TIP3P) (8000 particles) models.

From Figure 8, we see that for the same X_{BE} the long-range part of $r^2 h(r)$ initially crosses zero at approximately the same separation, r_{cross} , for both CH_3-O_W and CH_3-CH_3 . For $r < r_{cross}$, the CH_3-O_W correlation function is negative (water densities are lower than the bulk value), and for CH_3-CH_3 it is positive (BE densities exceed that of the bulk). This behavior is entirely consistent with the existence of BE-rich, water-poor aggregates, and the r_{cross} values provide some measure of the aggregate size. It is not completely clear how to physically interpret r_{cross} , because the rdf average contributions from BE molecules in all solution environments. Nevertheless, we might expect the positive CH_3-CH_3 correlations, and the negative CH_3-O_W correlations, to persist farthest from the origin, if the BE molecule at the origin is located near the center of a BE aggregate. If we further assume that BE aggregates are on average spherical in shape, then r_{cross} can be viewed as a crude estimate of the aggregate radius. From Figure 8, we obtain r_{cross} values of ~ 18 , ~ 26 , ~ 31 , ~ 33 , and $\sim 42 \text{ \AA}$ for $X_{BE} = 0.005$, 0.01 , 0.02 , 0.03 , and 0.04 , respectively. It is interesting to observe that the aggregate size grows rapidly between $X_{BE} = 0.005$ and 0.02 , remains nearly constant between 0.02 and 0.03 , and then shows some further growth between 0.03 and 0.04 .

As noted in the Introduction, there have been a number of studies using light scattering^{41–47} and SANS^{12,48,49} experiments aimed at probing the existence and size of aggregates in BE–water solutions. The experimental size estimates are also based on the assumption of spherical aggregates, and in general, for comparable concentrations and temperatures, the radii reported are in qualitative accord with our estimates based on r_{cross} . For example, at $\sim 300 \text{ K}$ and $X_{BE} = 0.048$, light-scattering experiments⁴³ give a hydrodynamic radius $r_H \approx 60 \text{ \AA}$, and at $X_{BE} = 0.04$, SANS⁴⁹ gives a radius of gyration $r_G \approx 42.6 \text{ \AA}$. Within a uniform spherical particle assumption, r_G and r_H obey the relationship⁴³ $r_G = (3/5)^{1/2} r_H$, so, given the concentration

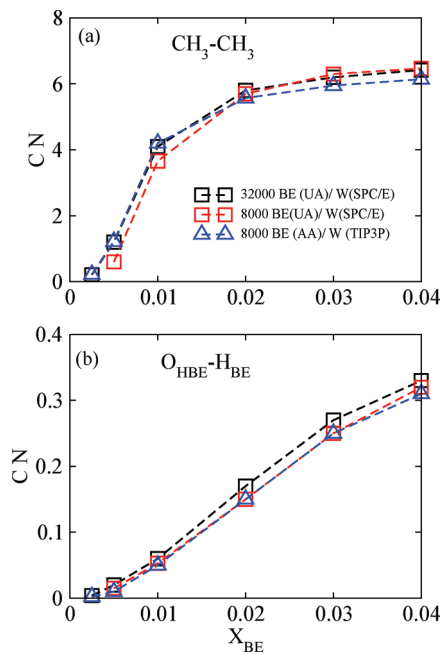


Figure 10. Selected BE–BE coordination numbers. Results are included for both the BE(GROMOS-UA)/water(SPC/E) (8000 and 32 000 particles) and the BE(CHARMM-AA)/water(TIP3P) (8000 particles) models.

difference, the light-scattering and SANS results are in good agreement with each other. They are also close to the r_{cross} value ($\sim 42 \text{ \AA}$) that we obtain at $X_{\text{BE}} = 0.04$. We note that there are also reports in the experimental literature^{38,45} of aggregates having $r_H \gtrsim 1000 \text{ \AA}$ for $X_{\text{BE}} < 0.02$. We can say nothing about this possibility because the largest number of particles (32 000) used in our simulations is too small by at least 3 orders of magnitude to probe correlations or aggregation on such very long length scales.

Further insight into association in BE–water solutions can be gained by examining coordination numbers (CN) given by

$$\text{CN} = \int_0^R \rho_\beta g_{\alpha-\beta}(r) 4\pi r^2 \, dr \quad (1)$$

where $\rho_\beta g_{\alpha-\beta}(r)$ is the product of a particular density and rdf, and the upper limit R is taken to be the first minimum in $g_{\alpha-\beta}(r)$. For example, if $\rho_{\text{wg}} \text{CH}_3-\text{O}_w(r)$ is used in eq 1, the average number of water oxygen atoms in the first coordination shell of a BE methyl group (the carbon of the methyl group for the all atom model) is obtained.

The BE–water coordination numbers are particularly revealing, and three of these designated CH₃–O_w (average number of water oxygen atoms in the first coordination shell of a BE methyl group), H_{BE}–O_w (average number of water oxygen atoms in the first coordination shell of a BE hydroxyl hydrogen), and O_{HBEBE}–H_w (average number of water hydrogen atoms in the first coordination shell of a BE hydroxyl oxygen), are shown in Figure 9. Results for both models and for two system sizes are plotted in the figure, and we note that the curves are very similar in all cases. From Figure 9a, we see that the number of water molecules in the first coordination shell of the BE methyl group drops very rapidly from a value of ~ 16.4 at infinite dilution to ~ 3.4 at $X_{\text{BE}} = 0.02$. This “dehydration” of the BE methyl group indicates that the hydrophobic “tails” of BE begin to associate at low concentration, the association increases quite sharply in the range

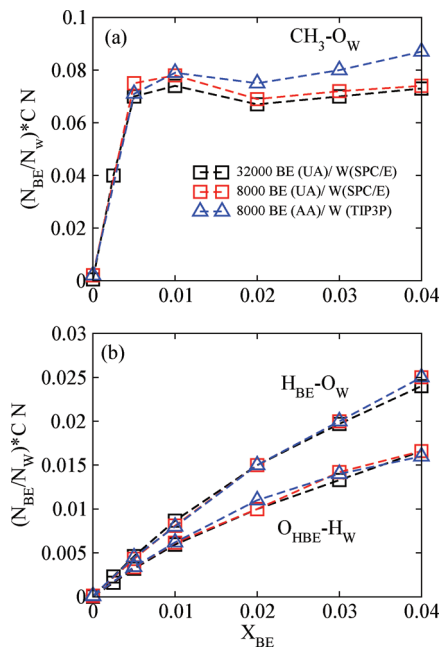


Figure 11. The function $(N_{\text{BE}}/N_w) \times \text{CN}$ for selected BE–water coordination numbers. Results are included for both the BE(GROMOS-UA)/water(SPC/E) (8000 and 32 000 particles) and the BE(CHARMM-AA)/water(TIP3P) (8000 particles) models.

$X_{\text{BE}} \approx 0.005 – 0.01$, and is near “complete” at $X_{\text{BE}} \approx 0.02$, with the coordination numbers changing only slowly for higher concentrations. The BE hydroxyl hydrogen and oxygen atoms also show some dehydration with increasing concentration, but the coordination number curves (Figure 9b) vary much more slowly than that of the methyl group. Taken together, the variation with concentration of the BE–water coordination numbers is consistent with the formation of loose micelle-like structures as revealed by the configurational snapshots (Figure 6).

The BE–BE coordination numbers are also instructive and results labeled CH₃–CH₃ (average number of BE methyl groups in the first coordination shell of a BE methyl group) and O_{HBEBE}–H_{BE} (average number of BE hydroxyl hydrogen atoms in the first coordination shell of a BE hydroxyl oxygen) are plotted in Figure 10. We note that the CH₃–CH₃ curve (Figure 10a) shows little indication of association at $X_{\text{BE}} = 0.0025$, but that the coordination numbers grow rapidly for $X_{\text{BE}} \approx 0.005 – 0.01$, and that the curve is tending to flatten out at $X_{\text{BE}} \approx 0.02$. This is completely consistent with the CH₃–O_w coordination numbers, and the aggregation picture discussed above. The O_{HBEBE}–H_{BE} coordination numbers (Figure 10b) also start near zero and increase with concentration, but more slowly than the CH₃–CH₃ values. This is consistent with the behavior of the H_{BE}–O_w and O_{HBEBE}–H_w curves discussed above and reflects the fact that the BE hydroxyl groups remain significantly hydrated as BE forms aggregates.

Additional insight can be gained from the BE–water coordination numbers by plotting $(N_{\text{BE}}/N_w) \times \text{CN}$, where N_{BE} and N_w are the numbers of BE and water molecules in the simulation at a particular concentration. $(N_{\text{BE}}/N_w) \times \text{CN}$ is the fraction of water molecules that are in the first coordination shell of at least one BE molecule. For example, if the CH₃–O_w coordination number is used, it is the fraction of water molecules in the first coordination of at least one BE methyl group. If there are no

significant changes in the coordination number with concentration, then, at low concentration, we would expect $(N_{BE}/N_W) \times CN$ to be a near linear function of X_{BE} . Results for CH_3-O_W , $\text{H}_{BE}-\text{O}_W$, and $\text{O}_{HBE}-\text{H}_W$ are shown in Figure 11. We note that, for $\text{H}_{BE}-\text{O}_W$ and $\text{O}_{HBE}-\text{H}_W$, the curves (Figure 11b) increase monotonically with X_{BE} showing little evidence of association, as we would expect from the weak concentration dependence of the relevant coordination numbers. In contrast, the influence of association is strikingly apparent in the CH_3-O_W plot (Figure 11a). For CH_3-O_W , the curve increases steeply to $X_{BE} \approx 0.005$, then slows abruptly, passes through a maximum at $X_{BE} \approx 0.01$, followed by a minimum at $X_{BE} \approx 0.02$. These features are a clear indication of association, marked by a rapid onset at $X_{BE} \approx 0.005$ and resulting in essentially fully formed aggregates at $X_{BE} \approx 0.02$.

IV. SUMMARY AND CONCLUSIONS

This paper reports a molecular dynamics investigation of association and microheterogeneity in 2-butoxyethanol–water solutions at low concentration ($X_{BE} \leq 0.04$). To ensure that our observations are not unduly biased by a particular model choice, simulations were performed with two different force fields, specifically, BE(GROMOS-UA)/water(SPC/E) and BE-(CHARMM-AA)/water(TIP3P), and both give qualitatively consistent results. Expecting at the outset that rather large systems would be necessary to accommodate BE aggregation, simulations were performed with 8000 and 32 000 particles, including both water and BE molecules. For correlations on molecular length scales, and related properties such as coordination numbers, both system sizes give near identical results. Also, qualitatively similar physical pictures emerge on the longer length scales associated with BE aggregation and microheterogeneity, but at the higher concentrations considered the larger system size is necessary to adequately accommodate the BE aggregates.

Apart from a qualitative examination of configurational snapshots, we have found two other methods to be useful in the detection and characterization of BE aggregation, and the attendant microheterogeneity. One approach is to consider the first coordination shell of the BE methyl group, in particular the concentration dependence of the water and methyl coordination numbers. The former shows the “dehydration” of the hydrophobic tail of BE upon association, and the latter indicates that the water molecules lost from the first coordination shell are being replaced by the hydrophobic parts of other BE molecules. We note that in our analysis we have focused for simplicity only on the BE methyl group, but similar conclusions are reached if one selects other parts of the hydrophobic tail of BE. Another indication of aggregation is given by the long-range behavior of the water–water, BE–water, and BE–BE pair correlation functions, plotted as $r^2h(r)$ for magnification purposes. When aggregation is present, these functions indicate density oscillations on length scales that are longer than any associated with single molecules. If one has a sufficiently large system, the pair correlation functions can both detect microheterogeneity and provide a measure of the length scales involved.

At very low concentration ($X_{BE} = 0.0025$), we find no indication of BE aggregation. Evidence is found of intramolecular hydrogen bonding, whereby the hydroxyl hydrogen and ether oxygen of the same BE molecule hydrogen bond to form five-membered ring structures, similar to those that have been reported in experimental studies of BE– CCl_4 solutions.⁶² Not

unexpectedly, at all concentrations we find hydrogen bonds between water and the hydroxyl group of BE, with BE acting both as a hydrogen donor and acceptor. Interestingly, there is only a very weak tendency for water to hydrogen bond to the ether oxygen of BE.

We first detect signs of association in the coordination numbers and correlation functions at $X_{BE} = 0.005$, but inspection of snapshots reveals only very loosely associated BE structures at this concentration. As the concentration is increased, the coordination numbers show rapid change up to $X_{BE} \approx 0.02$, followed by much slower variation at higher concentrations. Thus, BE association appears to begin at $X_{BE} \approx 0.005$ and to result in “fully formed” aggregates at $X_{BE} \approx 0.02$. Snapshots at $X_{BE} \approx 0.02$ show reasonably well-defined BE aggregates that could be described as micelle-like. We note that aggregation near $X_{BE} \approx 0.02$ has been reported in many experimental studies, and that our snapshots match the qualitative description that is often given of the BE aggregates. Our estimates of the size of the BE aggregates are also consistent with the estimates obtained from light-scattering and SANS experiments.^{43,44}

As a final observation, we note that it is now possible to simulate model aqueous systems sufficiently large to investigate aggregation and microheterogeneity on length scales of a few nanometers. The BE–water solutions considered here are perhaps simpler to study than many other aqueous systems, because the BE aggregates are well enough defined to be easily spotted in configurational snapshots. This is not always the case, but on the basis of the present BE–water example, we expect that the long-range behavior of the pair correlation functions might prove useful in detecting microheterogeneity in systems with less obvious aggregates.

■ AUTHOR INFORMATION

Corresponding Author

*E-mail: patey@chem.ubc.ca.

■ ACKNOWLEDGMENT

We thank Dr. A. Perera and Dr. Y. Koga for many interesting discussions. The financial support of the Natural Science and Engineering Research Council of Canada is gratefully acknowledged. This research has been enabled by the use of WestGrid and Compute/Calcul Canada computing resources, which are funded in part by the Canada Foundation for Innovation, Alberta Innovation and Science, BC Advanced Education, and the participating research institutions. WestGrid and Compute/Calcul Canada equipment is provided by IBM, Hewlett-Packard, and SGI.

■ REFERENCES

- (1) Koga, Y. *Solution Thermodynamics and its Application to Aqueous Solutions*; Elsevier: Amsterdam, The Netherlands, 2007; Chapters V and VI, and references therein.
- (2) Roux, G.; Roberts, D.; Perron, G.; Desnoyers, J. E. *J. Solution Chem.* **1980**, *9*, 629–647.
- (3) Smith, S.; Wiseman, P.; Boudreau, L.; Marangoni, G.; Palepu, R. *J. Solution Chem.* **1994**, *23*, 207–222.
- (4) Koga, Y.; Westh, P.; Moriya, Y.; Kawasaki, K.; Atake, T. *J. Phys. Chem. B* **2009**, *113*, 5885–5890.
- (5) Yoshida, K.; Baluja, S.; Inaba, A.; Koga, Y. *J. Chem. Phys.* **2011**, *134*, 214502–1–5.

- (6) Subramanian, D.; Ivanov, D. A.; Yudin, I. K.; Anisimov, M. A.; Sengers, J. V. *J. Chem. Eng. Data* **2011**, *56*, 1238–1248 and references therein.
- (7) Iwasaki, K.; Fujiyama, T. *J. Phys. Chem.* **1977**, *81*, 1908–1912.
- (8) Schmitz, J.; Belkoura, L.; Woermann, D. *J. Chem. Phys.* **1994**, *101*, 476–479.
- (9) Bowron, D. T.; Finney, J. L.; Soper, A. K. *J. Phys. Chem. B* **1998**, *102*, 3551–3563.
- (10) Dixit, S.; Crain, J.; Poon, W. C. K.; Finney, J. L.; Soper, A. K. *Nature* **2002**, *416*, 829–832.
- (11) D'Arrigo, G.; Giordano, R.; Teixeira, J. *Phys. Scr.* **1992**, *T45*, 248–250.
- (12) D'Arrigo, G.; Giordano, R.; Teixeria, J. *Eur. Phys. J. E* **2003**, *10*, 135–142.
- (13) Kusalik, P. G.; Lyubartsev, A. P.; Bergman, D. L.; Laaksonen, A. *J. Phys. Chem. B* **2000**, *104*, 9533–9539.
- (14) Lee, M. E.; van der Vegt, N. F. A. *J. Chem. Phys.* **2005**, *122*, 114509–1–13.
- (15) Fornili, A.; Civera, M.; Sironi, M.; Fornili, S. L. *Phys. Chem. Chem. Phys.* **2003**, *5*, 4905–4910.
- (16) Paul, S.; Patey, G. N. *J. Phys. Chem. B* **2006**, *110*, 10514–10518.
- (17) Laaksonen, A.; Kusalik, P. G.; Svishchev, I. M. *J. Phys. Chem. A* **1997**, *101*, 5910–5918.
- (18) Dougan, L.; Bates, S. P.; Hargreaves, R.; Fox, J. P.; Crain, J.; Finney, J. L.; Réat, V.; Soper, A. K. *J. Chem. Phys.* **2004**, *121*, 6456–6462.
- (19) Perera, A.; Sokilic', F. *J. Chem. Phys.* **2004**, *121*, 11272–11282.
- (20) Zoranic', L.; Mazighi, R.; Sokilic', F.; Perera, A. *J. Chem. Phys.* **2009**, *130*, 124315–1–11.
- (21) Perera, A.; Zoranic', L.; Sokilic', F.; Mazighi, R. *J. Mol. Liq.* **2011**, *159*, 52–59.
- (22) Mijakovic', M.; Kežić', B.; Zoranic', L.; Sokilic', F.; Asenbaum, C.; Pruner, C.; Wilhelm, E.; Perera, A. *J. Mol. Liq.* **2011**, *164*, 66–73.
- (23) Roney, A. B.; Space, B.; Castner, E. W.; Napoleon, R. L.; Moore, P. B. *J. Phys. Chem. B* **2004**, *108*, 7389–7401.
- (24) Roux, G.; Perron, G.; Desnoyers, J. E. *J. Phys. Chem.* **1978**, *82*, 966.
- (25) Roux, G.; Perron, G.; Desnoyers, J. E. *J. Solution Chem.* **1978**, *7*, 639–654.
- (26) Chiou, D.-R.; Chen, S.-Y.; Chen, L.-J. *J. Chem. Eng. Data* **2010**, *55*, 1012–1016.
- (27) Douheret, G.; Pal, A. *J. Chem. Eng. Data* **1988**, *33*, 40–43.
- (28) Elizalde, F.; Gracia, J.; Costas, M. *J. Phys. Chem.* **1988**, *92*, 3565–3568.
- (29) Yano, F. Y. *J. Chem. Phys.* **2002**, *116*, 8093–8096.
- (30) D'Angelo, M.; Onori, G.; Santucci, A. *Chem. Phys. Lett.* **1994**, *220*, 59–63.
- (31) Koga, Y. *J. Phys. Chem.* **1991**, *95*, 4119–4126.
- (32) Siu, W.; Koga, Y. *Can. J. Chem.* **1988**, *67*, 671–676.
- (33) Hvilsted, A.; Koga, Y. *Thermochim. Acta* **1993**, *228*, 39–46.
- (34) Koga, Y.; Siu, W.; Wong, T. Y. H. *J. Phys. Chem.* **1990**, *94*, 3879–3881.
- (35) Davis, M. I.; Molina, M. C.; Douheret, G. *Thermochim. Acta* **1988**, *131*, 153–170.
- (36) Douheret, G.; Pal, A.; Davies, M. I. *J. Chem. Soc., Faraday Trans. 1* **1989**, *85*, 2723–2736.
- (37) Lara, J.; Desnoyers, J. E. *J. Solution Chem.* **1981**, *10*, 465–478.
- (38) Kato, S.; Jobe, D.; Rao, N. P.; Ho, C. H.; Verral, R. E. *J. Phys. Chem.* **1986**, *90*, 4167–4174.
- (39) Arikawa, T.; Nagai, M.; Tanaka, K. *Chem. Phys. Lett.* **2009**, *477*, 95–101.
- (40) Mallamace, F.; Micali, N.; D'Arrigo, G. *Phys. Rev. A* **1991**, *44*, 6652–6658.
- (41) Ito, N.; Saito, K.; Kato, T.; Fujiyama, T. *Bull. Chem. Soc. Jpn.* **1981**, *54*, 991–997.
- (42) Ito, N.; Fujiyama, T.; Udagawa, Y. *Bull. Chem. Soc. Jpn.* **1983**, *56*, 379–385.
- (43) D'Arrigo, G.; Mallamace, F.; Micali, N.; Paparelli, A.; Teixeira, J.; Vasi, C. *Prog. Colloid Polym. Sci.* **1991**, *84*, 177–183.
- (44) Micali, N.; Trusso, S.; Vasi, C.; Mallamace; Lombardo, D.; Onori, G.; Santucci, A. *Phys. Rev. E* **1995**, *51*, 2349–2355.
- (45) Bender, T. M.; Pecora, R. *J. Phys. Chem.* **1988**, *92*, 1675–1677.
- (46) D'Arrigo, G.; Mallamace, F.; Micali, N.; Paparelli, A.; Vasi, C. *Phys. Rev. A* **1991**, *44*, 2578–2587.
- (47) Quirion, F.; Magid, L. J.; Drifford, M. *Langmuir* **1990**, *6*, 244–249 and references therein.
- (48) D'Arrigo, G.; Teixeira, J. *J. Chem. Soc., Faraday Trans. 1* **1990**, *86*, 1503–1509.
- (49) Yoshida, K.; Yamaguchi, T.; Otomo, T.; Nagao, M.; Seto, H.; Takeda, T. *J. Mol. Liq.* **2005**, *11*, 125–131.
- (50) Castillo, R. C.; Dominguez, H. C.; Costas, M. *J. Phys. Chem.* **1990**, *94*, 8731–8734.
- (51) Berendsen, H. J. C.; Grigera, J. R.; Straatsma, T. P. *J. Phys. Chem.* **1987**, *91*, 6269–6271.
- (52) Oostenbrink, C.; Villa, A.; Mark, A. E.; van Gunsteren, W. F. *J. Comput. Chem.* **2004**, *25*, 1656–1676.
- (53) Bjelkmar, P.; Larsson, P.; Cuendet, M. A.; Hess, B.; Lindahl, E. *J. Chem. Theory Comput.* **2010**, *6*, 459–466.
- (54) Jorgensen, W. L.; Chandrasekhar, J.; Madura, J. D.; Impey, R. W.; Klein, M. L. *J. Chem. Phys.* **1983**, *79*, 926–935.
- (55) Berendsen, H. J. C.; van der Spoel, D.; van Drunen, R. *Comput. Phys. Commun.* **1995**, *91*, 43–56.
- (56) Hess, B.; Kutzner, C.; van der Spoel, D.; Lindahl, E. *J. Chem. Theory Comput.* **2008**, *4*, 435–447.
- (57) Darden, T.; York, D.; Pedersen, L. *J. Chem. Phys.* **1993**, *98*, 10089–10092.
- (58) Essmann, U.; Perera, L.; Berkowitz, M. L.; Darden, T.; Lee, H.; Pedersen, L. G. *J. Chem. Phys.* **1995**, *103*, 8577–8592.
- (59) Bussi, G.; Donadio, D.; Parrinello, M. *J. Chem. Phys.* **2007**, *126*, 014101–1–7.
- (60) Berendsen, H. J. C.; Postma, J. P. M.; van Gunsteren, W. F.; DiNola, A.; Haak, J. R. *J. Chem. Phys.* **1984**, *81*, 3684–3690.
- (61) Hess, B.; Bekker, H.; Berendsen, H. J. C.; Fraaije, J. G. E. M. *J. Comput. Chem.* **1997**, *18*, 1463–1472.
- (62) Prabhumirashi, L. S. *J. Chem. Soc., Faraday Trans. 2* **1978**, *74*, 1567–1572.